Biomedical Wellness Standoff Screening by Unsupervised Learning

Harold H. Szu[a], Charles Hsu[b], Philip Hoekstra[c], Jerry Beeney[e],
[a]George Washington Univ. Wash DC and Army NVESD, Ft. Belvoir VA 22060.
[b]Trident Systems Inc., Fairfax Virginia 22030;[c]Therma-Scan Inc. Birmingham, MI; [e]FLIR, Boston MA

Abstract

Biomedical Wellness (BMW) surveillance system may become indispensible in public health riding on four confluent trends: (i) The surge of retirement waves of WWII baby boomers; (ii) The longevity of the seniors, thanks to 3 decades steady NIH budgets~$23B per year; (iii) The economic melting down is exasperating resources for entitlements; (iv) The emergent Next Gen Internet having the last mile challenges solved entirely and friendly with IT wired and wireless delivery system, thanks to DoD/DARPA pioneer and numerous entrepreneurs visionary efforts. To be effective in job re-creation in current economic slag, BMW needs a jump start, WH/HHS should establish a balanced investment policy in health care, not just to illness but to wellness, and a BMW blue ribbon panel (BMWbrp), which must be, however, independent of NIHbrp, recommending additional resources, say $5B budget for BMW infrastructure building that will surely create new jobs to prepare badly needed geriatric caretakers. Being governmental investment, the BMWbrp must come back with an upward-conversion compatible infrastructure Blue-Print, version#1, an open architecture of standard interfaces, workable with distributed data bases and programming languages. The infrastructure must be simple, transparent, scalable, to leverage with a win-win-win (senior) CRADA from the private investments worldwide, e.g. from the insurance companies and home security companies, etc. that can further attract senior community center BOT. To start whenever the rubber meets the road, we shall enlist the military infrastructure, their sensors suite located in DoD & DHS labs supported with their affiliated contractors and universities. However, the down selections should be done under open bids, oversight by BMWbrp, under HHS $5B budget, to translate their sophisticated military persistent and precision surveillance know-how technology to watch out, no longer the enemy of USA but also, the enemy of mankind, the malicious microorganisms and disorders. The degree of friendliness must be demanded and measured by the standoff methodology such as 4 nones: noninvasive, noncontact, and none-stop-to-measure, in this order.

Since the regulatory red tapes are historically targeted primarily at drug treatment of disease analysis in three phases progressions, there is no category or direct regulation rules for BMW investigations. Avoiding legal complication, one may wish to collaborate initially with the Far East as AFOSR/AOARD did well with their category IRB/PCF rules, because the BMW is a BMW, no matter where and who there are seniors. To facilitate this purpose, one may create BMW phase zero feasibility study worldwide, say as an earmark of US annul contribution to WHO, which would be a Middle East peace dividend for a global village Marshall Plan. All PI's and inventors worldwide can test their own gadgets in these and other federal labs to serve three parties well, at least in one of the following resolution scales: (i) **the users** (seniors of a family, a large community retirement or senior center, Desert Storm return PDS veterans, etc) to be monitored; (ii) **the caretakers** including home visit aids, nurses and physicians, and (iii) **the nerve center** including PC and/or data bases, and 6W searching engine with 3W hub linked to US CDC, UN WHO in all regions on Earth. Thus, a smart daily user-friendly screening and diagnostics is ideal to read, analyze and tabulate both physiological and mental wellness signs in a household PC hub.

We illustrate such an end unit of the smart BMW sensor web, in order to capture early malign tumors by means of a doublet of two commercial FLIR cameras, emulating the Army one cryogenic camera for two passive infrared spectral bands called the 3rd Gen FLIR. The twin FLIR cameras must first solve, not without errors, the 3D-subject 2D-projection correspondence challenge, and then the pair spectral vector per pixel becomes amenable to a patented unsupervised, and thus un-cohort-bias, smart learning algorithm called the Blind Sources (malign vs. benign) Separation (BSS). To entice the cost-reduction of the 3rd Gen FLIR camera development, besides the current modest success of breast cancer watcher, we need join force in dual usages, namely watching noninvasively over potential skin cancers of return sun-over-exposure soldiers, and watching covertly the distant biometric surveillance by a passive facial vein map against terrorist attack.

Keywords: Biomedical Wellness, infrared spectral band camera, malign tumors careening, home care system.

1. INTRODUCTION

A true anecdote story of low-tech BMW began with a low-cost night-vision fish-eye-video camera installed in all 100 senior homes, which was initially meant to pay the respect to the seniors' feeling of potential privacy invasion by high-definition day-night videotaping. Never mind about the real course of the decision, the cost, the privacy, or the size of image data basis, the fact of the matter was, after 2 years, the home care program had saved a bundle. Caretakers had eliminated 25% senior no-show incidences that had saved enormous manpower maintaining the same QOS with the modest cost of a simple plug-in code in their cell phones. The program had serendipitously discovered the early behavior symptoms of ***Alzheimer*** *disease*, namely midnight random walks, which is amenable to a low cost early intervention treatment. In so doing, it had preserved those senior's QOL--better night sleeps, contributing better day hours to volunteer services to other less fortunate. Furthermore, this cascade of a good deed breeding another good deed will save senior mental health expenditure, the helper and the 'helpee'---their self-esteem, and other exurban societal expenditure of the prescription drugs and three-shift caretakers, in the case of early deterioration of acute dementia. Unfortunately the chances are very high to any late discovered seniors. Our motto said well; "you don't just, get what you pay for, if you do good business, you'll do well", which has once again verified the common sense of BMW thesis: "a stitch in time saves nine." The end of BMW excursion.

The US Army is developing 3rd Gen *Forward Looking Infrared (FLIR)* sensor technology to maintain the overarching advantage that the military forces have enjoyed in night vision dominance in the Mid East conflict. The simplest implementation of this technology has the two spectral bands operating dependently, in the sense of Planck thermal radiation spectrum intensity relationship. The spontaneously thermal emission spectral ratio of a warm human body becomes independent of the environmental effect. There are about 10% mid IR photons versus 90% Long IR photons whose ratio index becomes robust in weak noise limit:

$$\text{spectral ratio per pixel } \rho(x,y,t) = \frac{\text{mid}+\text{noise}}{\text{long}+\text{noise}} = \frac{\frac{\text{mid}}{\text{noise}}+1}{\frac{\text{long}}{\text{noise}}+1} = \begin{cases} 0 & \text{noise} \ll 10\% \text{ in colder background} \\ 1 & \text{noise} \gg 10\% \text{ in hotter background} \end{cases} \quad (1)$$

This dual spectral image will be vital to BMW watch of the spectral ratio $\rho(x,y,t)$ whether or not it exceeds individual safety range. Alternatively, the camera spectral bands can be independently gain controlled and operated with the user selecting the band that provides the "best" imagery. That is the basic operational scenario assumed for this design of camera. Other more sophisticated uses of the multiband capability are envisioned, e.g., dual-band image fusion, spectral anomaly detection, new spectral *Aided Target Recognition (AiTR) such as single-pixel Blind Sources Separation (BSS)*, Higher Order Statistics ICA, etc., that could dramatically increase the 3rd Gen *FLIR* sensor effectiveness. The cost may come down, as more civilian usages could be documented. Thus, we discuss another dual-band application for the biomedical wellness (BMW) spectral imageries fusion for AiTR skin melanoma and other malign tumors for desert sun over-exposure high risk return war fighters and their households. Another popular applications in BMW may help reveal vein map dynamics and reduce the cost of the 3rd Gen FLIR, that are beneficial to PM FLIR and all other military and civilian players including the human signature exploitation for physiology behavior useful for the standoff biometric required for Combat Search & Rescue (C-SAR) requirement: the authentication and the situation assessment.

A 3rd Gen *FLIR* sensor is defined as a cryogenically cooled multiband *MWIR/LWIR* thermal *Focal Plane Array (FPA)* imager used for target acquisition. The multiband aspect of the 3rd Gen FLIR will typically involve imaging of two spectral regions simultaneously on the same *FPA* to provide accurately registered simultaneous or near simultaneous imagery. The primary technology for multiband infrared detectors is that of *Mercury Cadmium Telluride (MCT)*, where two and three bands have been detected on a focal plane by layering the *MCT* with different *stochiometric* variations[1,2].

Simultaneous two-color *FPAs* have two *Indium* bumps per pixel at 50 μm for simultaneous two-color pixel. Pixel size is the most important factor for achieving affordable Third-Generation systems. Simultaneous two-color pixels have two indium bump connections per pixel to allow readout of both color bands at the same time. Advanced etching technology is required in order to meet the challenge of shrinking the pixel size to 20 μm.

2. PHYSICS APPROACH

The application of thermal imaging to breast cancer detection is traceable back in time to the earliest medical writings of ancient *Egypt* and *Mesopotamia*. Different types of "*fevers*" were described and their evaluation was limited to the touch of their physicians' hands. The Greek physicians of the classical age described the innovative method of applying thin slurry of mud to their patients' skin and observed differential drying to indicate abnormal patterns of heat and cold. The *Hippocrates corpus*, the "Father of Medicine", canonized '*Calor*' as a cardinal sign of disease and wrote "wheresoever's excessive heat or cold, there disease is to be found". Instrumentation was, however, lacking until the development of a '*thermoscope*', a primitive and un-calibrated thermometer by *Galileo* and its application to medical practice in the Fourteenth Century by *Boerhaaven*. It was William Hershel that first imaged thermal energy by developing an '*evaporograph*' in the Fifteenth Century and the first practical means of imaging thermal energy came as recently as the middle of the Twentieth Century with the development of an electro-optical scanner. It was *Ray Lawson*, a gynecologist at *McGill* University that applied this new device to Medicine and, specifically, to the detection of breast cancer.

We have applied the Planck "Blackbody" irradiation spectrum as a family of temperature-displaced Gaussian Bell-shape distributions, Wien's displacement rule, to the BMW spontaneously irradiation as a sensible model of human "graybody" spectrum distribution. Without knowing the heat transfer system impulse response function, we wish to solve the ill-posed inverse sources (malign versus benign) problem, called the blind sources separation (BSS) pixel by pixel, by the minimization of each pixel unknown Helmholtz isothermal free energy as the local equilibrium condition.

We further assume each pixel free energy of Helmholtz H to be analytical in each pixel I/O, whose input spectral vector per pixel is X= (MWIR, LWIR) and output feature vector per pixel is S=(malign s_1, benign s_2). Then we can expand the unknown energy in the weak signal sources limit in terms of Taylor series of unknown features estimated from the spectral vector data: $\sum_j W_{ij} X_j = s_i$ and vice versa $\sum_j A_{ij} s_j = X_i$ keep the linear order term neglecting the second order estimation errors $O(\Delta s^2)$, without knowing the mixing impulse response function matrix [A], nor the de-mixing inverse matrix [W]=[A]$^{-1}$. In other words, given numerous possible ill-posed inverse solutions of BSS, one will choose the mostly likely locally equilibrium one at the local minimum free energy pixel by pixel.

$$\min.\, H \equiv E(I/O) - T_o S = E_o + \sum (\partial E/\partial s_i)[\sum_j W_{ij} X_j - s_i^{(o)}] + O(\Delta s^2) - T_o K_B(-s_1 \log s_1 - s_2 \log s_2), \quad (2)$$

where use is made of the Shannon scalar entropy *S* for two components and the Lagrange constraint parameter $(\partial E/\partial s_i) \equiv \mu_i$ which is the *internal energy slope teacher* determined self-consistently by Lagrange in the general physics variational minimization. This is what we call the *unsupervised learning* in the sense of "*unlabelled data classifier*", a la *Duda and Hart* classical definition of statistical pattern recognition.(US PTO# 7,355,182; & #7,366,564)

Theorem 1: Exact solution for two components malign and benign is possible because the minimum Helmholtz free energy has three conditions for three unknowns as follows:

Proof:

$$H_p \equiv E_p - T_p S_p;$$

$$H_p = 0; \qquad E_p = T_p S_p \qquad (3)$$

$$\frac{dH}{ds_1} = 0 \qquad \frac{dE_p}{ds_1} = T_p \frac{dS_p}{ds_1} \qquad (4)$$

where Shannon & Boltzmann define the entropy S_p

$$S_p = -s_1 \log s_1 - (1-s_1)\log(1-s_1)$$

$$\frac{dS_p}{ds_1} = -\log s_1 - \frac{s_1}{s_1} + \frac{1-s_1}{1-s_1} + \log(1-s_1) = \log(1-s_1) - \log s_1$$

$$LHS = E_p / K_B = slope\ s_1 + intercept = RHS$$

$$RHS = T_o \frac{dS_p}{ds_1} s_1 + E_o^* = T_p \{\log(1-s_1) - \log s_1\} s_1 + E_o^* / K_B$$

$$LHS / K_B T_p = S_p = -s_1 \log s_1 - (1-s_1)\log(1-s_1) =$$

$$RHS = \{\log(1-s_1) - \log s_1\} s_1 + E_o^* / K_B T_p$$

$$E_o^* / K_B T_p = -\log(1-s_1^*)\ \ malign\ \ s_1^* = 1 - \exp(-\frac{E_o^*}{K_B T_p}) \qquad (5)$$

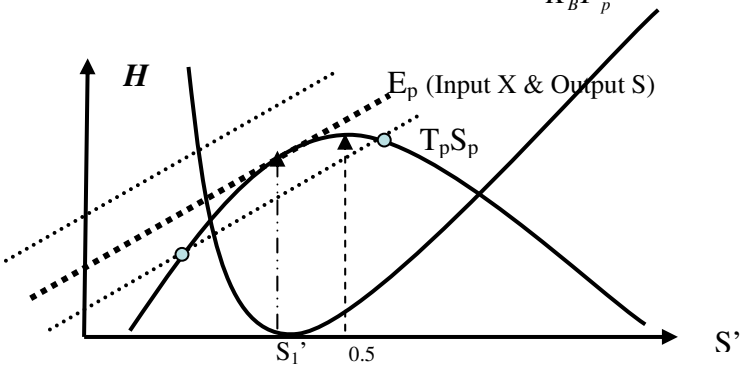

Fig. 1 We postulate a min Helmholtz free energy as the linear I/O info energy $\Delta E_p = \mu\{[W]X_p - S_p\} = \lambda\{[A]S_p - X_p\} = LMS$, *if* $\mu = [W]X_p - S_p]$ and the max entropy give wrong solutions $s_2' = 1 - s_1' = 0.5$

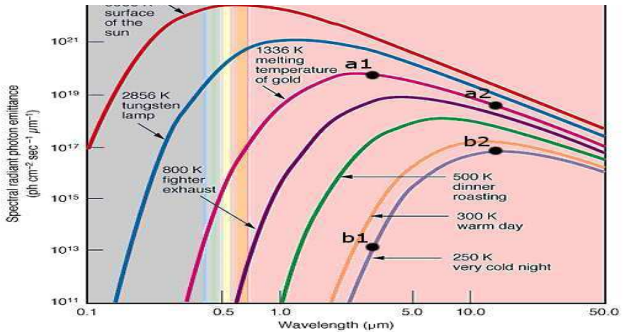

Fig.2 Physicist Planck measured the temperature–dependent thermal spectrum which, for a non-absolute-zero temperature object, has laid foundation of quantum physics.

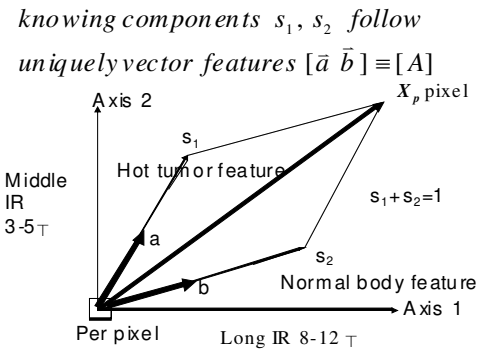

Fig. 3 Real Positive Subspace uniquely determines Planck Spectrum feature vectors (*a, b*) by means of a vector parallelogram if the percentage is given in Fig.1.

All these processing could be processed and given a second opinion at a distant without additional cost. This is because of NGI. Meanwhile, IT promises a quadruple pipeline broadband 32 bytes backbone that will enjoy the build-in privacy, secured, always-on, everywhere, universal, ubiquitous, seamless encompassing all.

3. PHYSIOLOGY APPROACH

There was an abundance of empirical evidence that linked regional *hyperthermia* with breast cancer, often as its first objective indication, but without any rationale for the mechanisms involved. In just the last twenty years, the role of *Nitric Oxide* as a potent regional *vaso-dilator*, produced in copious quantities by pre- and cancerous cells as well as the functionally defective structure of *neo-angiogenic* blood vessels have been recognized as the principal mechanisms that are responsible for an *unregulated perfusion of core-body temperature blood* into the proximity of the abnormal cells in the breast. Further, the mechanism directing this heat to the skin surface can be described by the principles of *Fournier's* Law that warmer irradiation eventually diffuse outwards to the colder ambient air where the cameras located. The two spectral density ratio may eliminate some of the environmental variability that may have plagued the pioneer work of single camera thermograph. Then, tracking over time allows one do better.

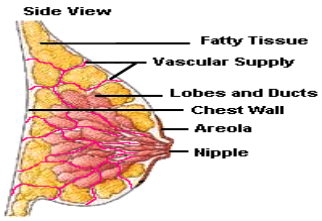

Fig. 4 Artist conception of a breast internal structure

To keep things simple, **breast cancers** emerge due to a combination of genetics, carcinogens, immune responses, hormones, and tissue composition. The breasts are composed of lobes, lobules, ducts, glands, and a high concentration of blood vessels and fat cells. Many of these tissues in the breast have receptors for the hormone estrogen, which makes them a target for the hormone's influence. Some of this is good and some bad. Of particular interest are the fat cells. Fat cells both produce and breakdown estrogen. The chemical breakdown reaction (aromatization) of estrogen produces carcinogenic (cancer causing) byproducts. As a result, the carcinogens affect the DNA of nearby cells which can cause them to mutate into cancers. Research has shown that some women's breasts are more susceptible than others to the effects of estrogen and its byproducts.

How Does the Cancer Grow? Once a normal cell begins to mutate (pre-cancerous tissue), its DNA is altered to allow for the onset of uncoordinated growth. To sustain the rapid growth of these pre-cancerous (and cancerous) cells, constant supply of nutrients is needed. In order to maintain this supply, the cells release chemicals into the surrounding area which keep existing blood vessels open, awaken dormant ones, and create new ones (**neo angiogenesis**). The rich vascular beds in the breast provide the conditions necessary for the growing tumor's needs.

How Can We Detect this Growth at its Earliest Stages? The ideal early warning system would detect both the pre-cancerous changes occurring in the breast and the first cancer cell formations. Digital Infrared Imaging (DII or Breast Thermography) has the ability to detect the chemical and blood vessel changes in pre-cancerous as well as cancerous breast tissue. Consequently, DII can be the first indicator that a cancer may be forming or present; and in many cases from **8-10 years before it can be detected by any other method.** The use of DII (Breast Thermography) as part of the frontline tests for early detection brings a great deal of good news for women.
Through the neo-angiogenesis effect we can detect the imminent danger passively by a dual IR spectral band camera, before the rapidly growth imbalance with nutrition supply may kill some cells, and left behind micro-calcification deposits, like spider webs, detectable by invasive X-ray mammograms change detection comparing the before with the after..

Our laboratory has interchangeably used mid (3-5μM) and long (9-12μM) instruments with thermal sensitivities better than 80 mK (NETD) and spatial resolution of 60 microRadians, usually in the form of a focal plane array of 320X256 for diagnostic breast cancer studies. We obtain two sets of three images; a frontal and two lateral views, approximately 60° off axis of the thorax, to feature the right and left breasts. Our analytic system has four components. (i) *The first* is a system of pattern recognition that evaluates the bilateral distribution of thermal features and the conformation of individual thermal features. (ii) *The second* evaluates bilateral temperature differentials. (iii) *The third*, and most innovative, evaluates the appropriate and adaptive response of the thermal features of both breasts to a standardized challenge. The physiologic challenge we use involves the immersion of both hands for one minute into a basin of water maintained at *11°C*, importantly, a temperature widely perceived as decidedly *cold but not painful*. This produces a *reflex vaso-constriction* of skin perfusion and an accompanying decrease in skin temperature: provided that the perfusion of any specific area is normally modulating under the control of the autonomic nervous system. This simple procedure is intended to differentially identify non-responding thermal features maintaining their high levels of blood perfusion due to the *functional-defective structure of neo-angiogenic vessels* or the *persistent vaso-dilatation* due to high levels of *Nitric Oxide*; both of which typify regional metaplasia and cancer. As any other physiologic response, this challenge procedure is closely controlled for strength and duration of the stimulus and the time of the imaging in order to evaluate the active phase of the *adaptive response*.

This physiologic challenge procedure has enabled us to differentially indicate malignant breast disease from other sources of heat on the surface of the breast, such as the hyper-perfusion that accompanies glandular hyperplasia of a pre-menstrual state, pregnancy or lactation; thereby significantly increasing the diagnostic specificity of thermology as a diagnostic screen for breast cancer. (iv) *The fourth* component of our analytic system involves the time-based evolution of the thermal patterns, emission levels or new and area specific defects in the response to our challenge procedure. As breast cancer is, generally, a positively progressive disease, we find that routine annual restudies, or sooner when only minor risk features are discerned, provides a useful means of differentiating artifact and personal variants (such as *arterial-venous shunts*) from the thermal features associated with malignant disease.

With our objective and quantitative analytic system, we believe that thermology better defines the adaptation of a scientific basis to what has been termed *thermograph*. Using our analytic system, the sensitivity of thermology as a diagnostic screen for breast cancer is near absolute (97-99%) and provides a high specificity (64-78%). Thermology is passive, non-contact and, in the context of screening for breast cancer, relatively inexpensive and able to effectively screen large numbers of women irrespective of their age or breasts' density.

4. IMAGE PROCESSING

In order to compare the single camera LWIR versus double cameras with LWIR and MWIR, we have adopted two comparable cameras made by the State of the Art 2nd Gen FLIR made by FLIR company in Boston. An identical general setup was used for both the MIR and LIR camera. Data was acquired using a 640x512 pixel InSb (Indium Antimonide) Mid-IR (3-5μm) and a 640x512 pixel Quantum Well Infrared Photon (QWIP) Long-IR (8-10μm) camera. Electric refrigeration was required to keep the Mid-IR camera cooled at 77°K after 5 minutes at a sensitivity (MRTD) of 0.018°K. Similarly, electric refrigeration was required to keep the Mid-IR camera cooled at 77°K after 5 minutes at a sensitivity (LRTD) of 0.03°K. Then, there are several modules of image processing which can do without in the 3rd Gen FLIR as follows:

The first challenge is that the images registration becomes spatially non-isoplanatic nature. This is because of the 3D stereo images prospectively projected onto 2D plane. This can be appreciated by the fact that the classical 2D affine transformation based of 3 correspondent control points gives rise to a poor result.

Affine transform is one of the solutions for data registration to align these dual camera sensor data into a common time or space coordinate system. Translation and rotation transforms are usually caused by the different orientation of the sensor, while scaling transform is the effect of change in altitude of the sensor. The sensor distortion or the viewing angle may cause stretching and shearing; the affine transform is a matured technology used to address more complex distortions. It is a linear coordinate transformation that consists of the elementary operations. Fig. 5 shows the basic transformations for data registration, and the general 2D affine transformation can be expressed as shown in Eq. (1).

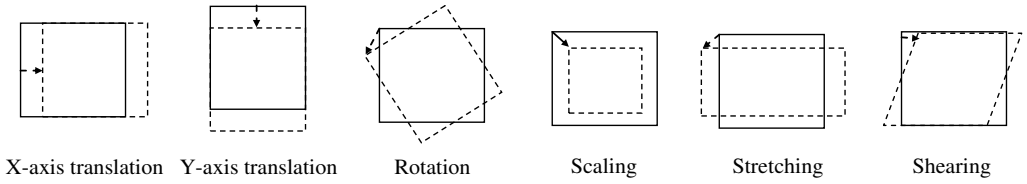

Fig.6. The basic transformations for data registration

$$\begin{bmatrix} x_2 \\ y_2 \end{bmatrix} = \begin{bmatrix} t_x \\ t_y \end{bmatrix} + \begin{bmatrix} a & b \\ c & d \end{bmatrix} \begin{bmatrix} x_1 \\ y_1 \end{bmatrix} \tag{6}$$

where $[x_2, y_2]^T$ is the new transformed coordinate of $[x_1, y_1]^T$, matrix of $\begin{bmatrix} a & b \\ c & d \end{bmatrix}$ can be the operations of rotation, scale, or shear, and $[t_x, t_y]^T$ is the translation. The rotation can be operated as $\begin{bmatrix} a & b \\ c & d \end{bmatrix} = \begin{bmatrix} \cos\theta & -\sin\theta \\ \sin\theta & \cos\theta \end{bmatrix}$; the scaling operation for both x and y axes can be expressed as $\begin{bmatrix} a & b \\ c & d \end{bmatrix} = \begin{bmatrix} S_x & 0 \\ 0 & S_y \end{bmatrix}$; and the shearing operation is represented by $\begin{bmatrix} a & b \\ c & d \end{bmatrix} = \begin{bmatrix} 1 & \alpha \\ 0 & 1 \end{bmatrix}$ or $\begin{bmatrix} a & b \\ c & d \end{bmatrix} = \begin{bmatrix} 1 & 0 \\ \beta & 1 \end{bmatrix}$.

However, this 2D affine transform can not solve the 3D stereo images from dual infrared camera. 3D affine transformations have been widely used in computer vision and particularly, in the area of model-based object recognition, and they can have involved different number of parameters involved:

- 12-parameter affine transformation (3D translation, 3D rotation, different scale factor along each axis and 3D skew) used to define relationship between two 3D image volumes. For instance, in medical image computing, the transformation model is part of different software programs that compute fully automatically the spatial transformation that maps points in one 3D image volume into their geometrically corresponding points in another, related 3D image volume[4].
- 9-parameter affine transformation (three translations, three rotations, three scales), can be used in reconstructing the relief and evaluating the geometric features of the original documentation of the cultural heritage by 3D modeling [5].
- 8-parameter affine transformation (two translations, three rotations, two scale factors and skew distortion within image space) to describe a model that transform 3D object space to 2D image space[6].

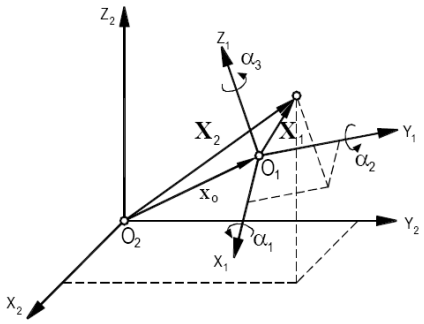

Fig.7 An example of 3D affine transformation

Our simulation experience shows that the 3D affine transform has difficulty to effectively register the stereo images due to the image distortion from the 3D imagery projection. In order to efficiently overcome this projection distortion, a dual-image registration using small regions of edge features is developed and proposed here to adaptively register small areas. This dual-image registration algorithm is demonstrated using the breast cancer data as follows.

The small-region and dual-image (long-wavelength infrared (LIR) and mid-wavelength infrared (MIR)) registration process contains a number of operations, including edge extraction, edge dilation, and object erosion. First of all, region of interest (ROI) must be selected. In this simulation, the LIR ROI is selected as a reference image which should be bigger. And the MIR LOI is smaller and will be registered to the LIR-ROI based on small regions. Next, the edge can be extracted using high-pass filters such as Mexican hat filter, Sobel filter, or odd Morlet filter. For implementation simplicity, a two-dimensional Sobel filter in equation (2) is applied to the dual-IR images. The thresholding operation is significant in the edge process. Thresholding may be different for the dual-IR images due different dynamic ranges of the IR images. An adaptive thresholding operation is needed to provide good estimated edge information on both IR images. The result of edge extraction using Sobel filter is illustrated on the top in Fig.3. The LIR ROI is shown on the left and the MIR ROI is on the right.

$$Soble_H = \begin{bmatrix} 1 & 1 & 1 \\ 0 & 0 & 0 \\ -1 & -1 & -1 \end{bmatrix}; \text{ and } Sobel_V = \begin{bmatrix} 1 & 0 & -1 \\ 1 & 0 & -1 \\ 1 & 0 & -1 \end{bmatrix} \quad (7)$$

Once the edge is extracted, the edge information will be dilated on its neighborhood. A dilation window should be big enough to form an object or a small region. However, if the dilation window is too big, it will generate too many redundant objects or small regions that will reduce the performance of registration and dissipate the computing resource on a number of redundant regions and objects. The dilation operation is demonstrated on the middle in Fig.3.

Erosion operation is to shrink the size of the objects from the outside of the objects. Similarly the erosion window has to be selected first to reduce the size of objects. The erosion window should be selected carefully. If the erosion window is too big, it will remove all the objects or regions created from the dilation operation. If the erosion window is too small, a number of redundant objects and regions will be processed such that it will reduce the performance and efficiency in the registration process. Our simulation experience shows that if the erosion window should be slightly small the dilation window, it will provide a better result. The erosion operation is illustrated on the bottom in Fig.3. It can be observed a number of regions or objects are extracted. These regions and objects will be masked with the normalized LIR and MIR images that are the templates for the registration.

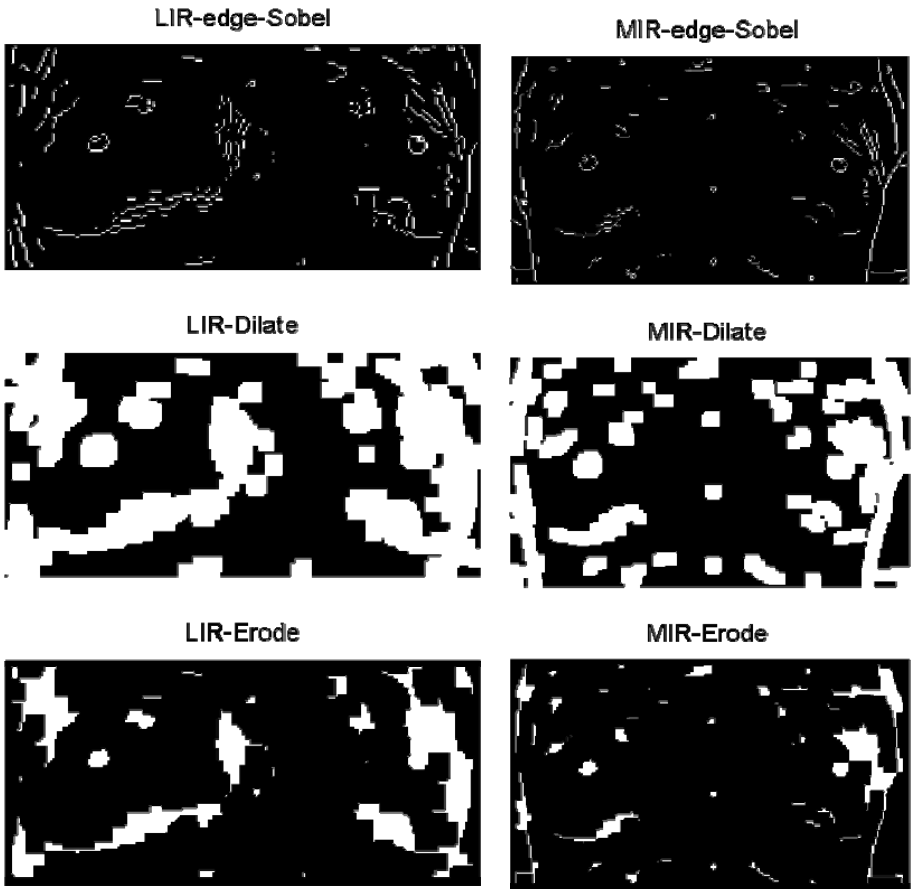

Fig.8 Three operations and demonstration of the small-region dual-IR image registration algorithm. (Edge extraction, dilation and erosion)

Once the eroded images are computed, the LIR-ROI and MIR-ROI images will be normalized and masked with the eroded images. The masked LIR-ROI is the reference image, which is processed block by block and registered to the MIR-ROI images. The sum of difference (SoD) of the blocked LIR-ROI and MIR-ROI will be calculated and compared. The index and position will be stored where the SoD is found. The MIR-ROI will be re-registered with the LIR-ROI when all the index and position with the minimum SoD. The SoD operation requires heavy computation resources. The spiral search with a specific threshold value is suggested here to reduce the computation complexity. Since every single block will obtain its own optimized match by calculating the SoD minimum, this mechanism can be used to adaptively resolve the image distortion of the affine transformation. The result is demonstrated in Fig.7, and the difference is displayed on the bottom on the right. The difference is normalized for the display purpose.

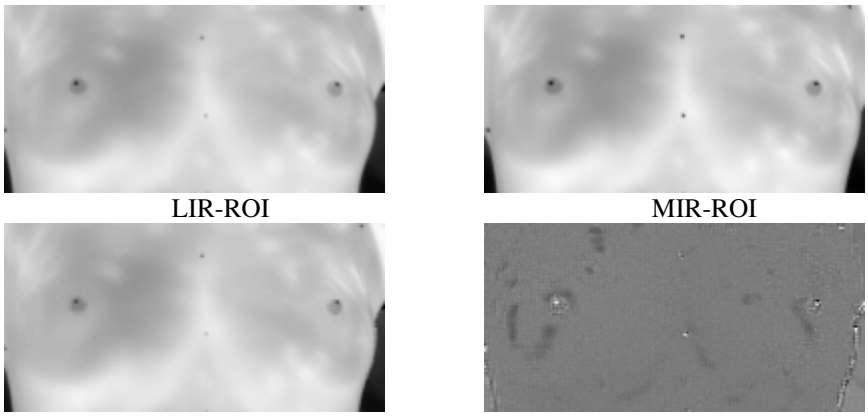

LIR-ROI MIR-ROI

Registered MIR-ROI Normalized Difference

Fig.9 Registration results. Massive breasts will have less successful results, causing sub-pixel inaccuracy affecting early detection at a single pixel level.

5. DUAL-BAND BMW BIOMETRIC ALGORITHMS

A dual-band BMW biometric algorithm is developed and illustrated by using a number of breast images. Theoretically, this algorithm is an unsupervised learning with equilibrium state energy [7]. For a point source, although the measurement at a specific pixel cannot be estimated using the average of its surroundings, the equilibrium state energy presents strong similarity with its neighboring pixels. Thus, the ground state energy E_0 from the neighboring pixels can be calculated to provide a good estimate. Due to the spatial variation of human body temperature, this ground state energy has to be determined within a local window of neighborhood. One difficulty is to decide the size of the neighborhood in which all pixels possess similar ground state energy, which varies from pixel to pixel. From geometric point of view, each point is a vector in a multidimensional space. If there is no target present in a neighborhood, then all these data vectors point to the same direction, which is the direction of the background signature. Then the angles between those vectors will be zero. Suppose there exists a sub-pixel target, one of the data vectors will depart from others and the angles are not zero any more. Quite obviously, the larger the fractional abundance of target, the further away this corresponding pixel departs from others, and the larger the angles. Based on these observations, we proposed to use the angle between data vectors as the measure of information energy E_o. This algorithm using unsupervised learning with equilibrium state energy is named "Exact Solution". Two algorithms called "Exact Solution Using Average Absolute Angle (ES-AAA)" and "Exact Solution Using Average Composite Angle (ES-ACA)" are derived and a number of simulations are demonstrated to provide more information of dual-band IR images.

In the ES-AAA algorithm, the dual-band images must be registered first using the registration algorithm described in section 5. And then every single pixel of the IR breast image has two components, MIR and LIR, that are represented as x- and y- coordinates respectively. And, the absolute angle can be obtained by averaging $tan^{-1}(MIR/LIR)$ of the 8 neighborhood excluding itself. Six cases of the IR breast images are studied and simulated. And the results are compared to the ground truth shown in Fig.5. And the ground truth of these patients is listed in Table 1. From the numerical analysis of the ES-AAA, it can be observed that the ES-AAA values are closed. This is due to the inappropriate wavelength ranges (3-5 μm and 8-10 μm). In the ES-ACA algorithm, the composite angle can be calculated by averaging the angles between the center vectors to 8 neighborhoods, which is displayed in Fig. 6.

Case15:

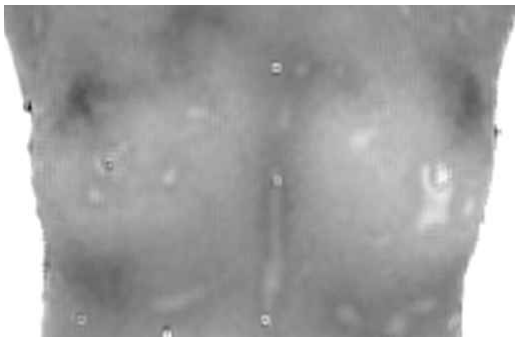

Case24:

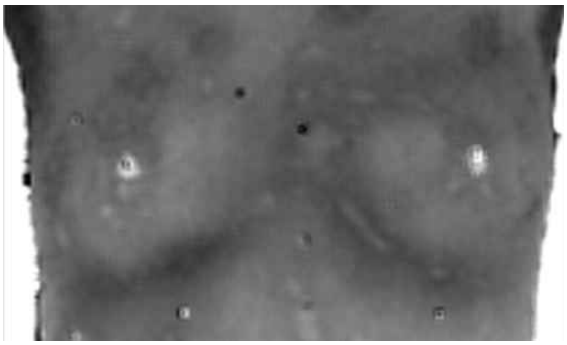

Case25:

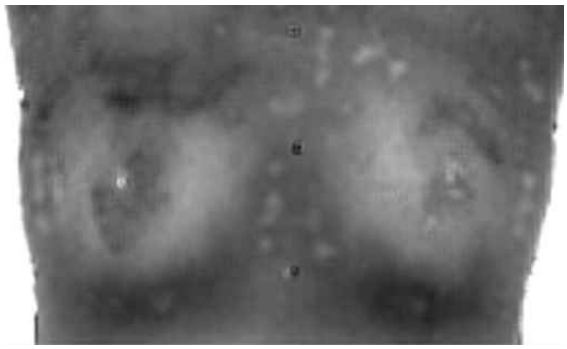

Case26:

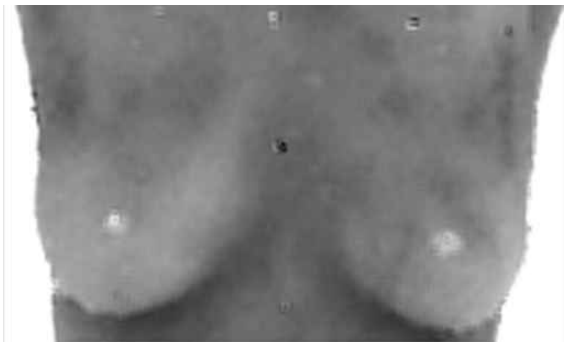

Case64:

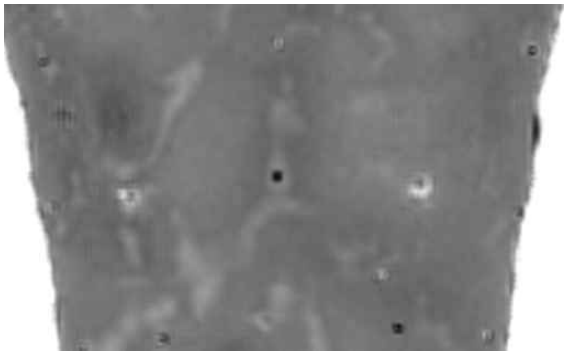

Case72:

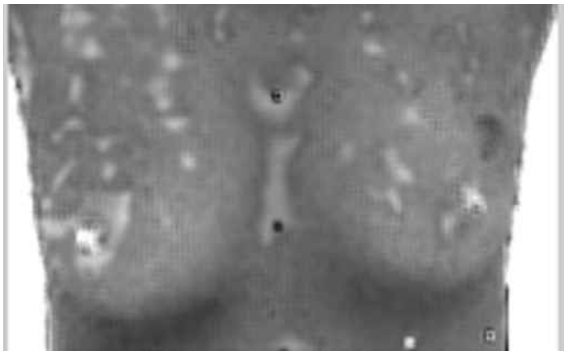

Fig.10. Case studies using the "Exact Solution Using Average Absolute Angle (ES-AAA)" versus "Exact Solution Using Average Composite Angle (ES-ACA)" Fig. 11.

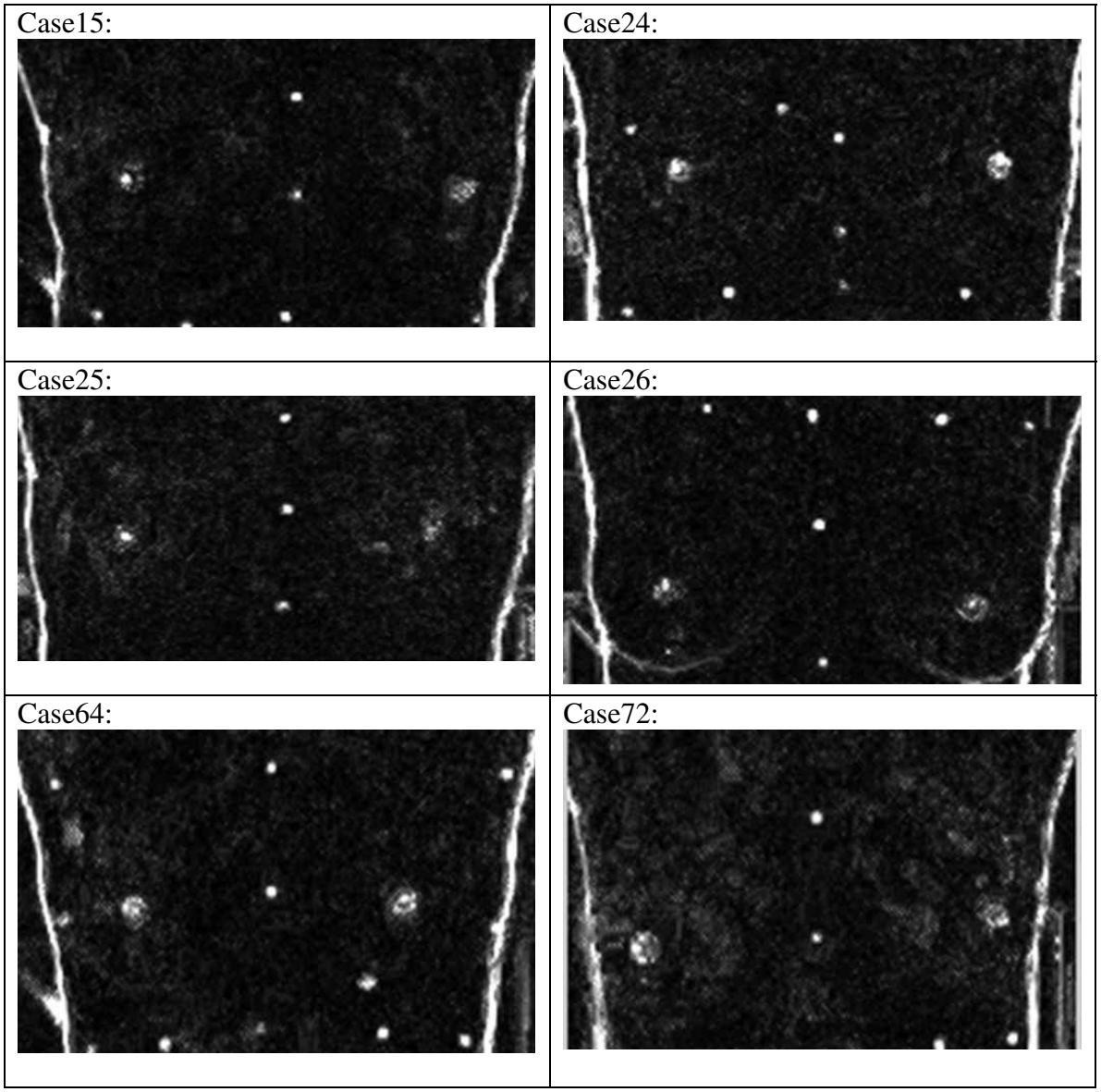

Fig.11. Case studies using the "Exact Solution Using Average Composite Angle (ES-ACA)"

Table 1: The ground truth of these six cases (patients). R x/y means the tumor is on the right side breast at 8 o'clock direction, and 2 cm from the nipple.

IR number	Operation result	TumorSize (Microscopy)	type	Tumor location in Ultrasound	Tumor size in Ultrasound
case15	R8/2	0.9*0.8*0.5	IDC	R10/3 R10.5/3 R10.5/3 R8/2 R12/4 R12/4	1.8*1.5 1.2 1.7*1.5 2.9*2.0 0.8 0.8*0.6
case24	R12/4	3.3*1.3	IDC	R12/4	2.7*1.7 (1.2*1.3)
case25	R10.5/4	2.8*1.6*1.5	IDC	R10.5/5 L5/0 L8.5/3	1.25*1.45 0.52*0.43 1.6*1.3
case26	L8/3	3*1.6	IDC	L8.5/3 L8.5/3	1.6*1.3 2.5*1.7
case64	R10/3	2.8*1.2*3.6	IDC	R10/3 R12/3	3.14*1.53 0.99*0.73
case72	L1/2	1.3*1.0	IDC	L1/2	1.2*0.8

The thermal infrared screening measures the indications of breast cancer associated with the angiogenesis effect, the formation of a blood supply to abnormal cells. The blood supply causes abnormal cells to respond differently from healthy cells to temperature changes. Abnormally reproducing breast cancer cells demand greater nutrition through increased blood supply, which therefore generate higher concentrations of heat in specific areas. From this sense, the problem of breast cancer detection is equivalent to detect the area of high concentration heat region and the intensity of the heat. The Plank radiation law[7] has shown that the high temperature drives the radiation curve to go toward top-left corner as illustrated in Fig. 2, where different curves correspond to the blackbody radiation of different materials at various temperatures. We wish the thermal infrared screening measures can distinguish the abnormal cells from normal ones in different environmental temperatures. In the experimental simulation, two LIR images are used. One is the regular LIR image, and another one is the LIR with cold treatment (namely challenge process). Once two LIR images are captured and registered, the LCNN (Lagrange Constraint Neural Networks) algorithm[8] was applied to decompose the IR images, and the results are demonstrated in Fig. 8.

LIR image after challenge (LIR05_07_2008_P2_4_A.csv)

LIR image before challenge (LIR05_07_2008_P2_4_A.csv)

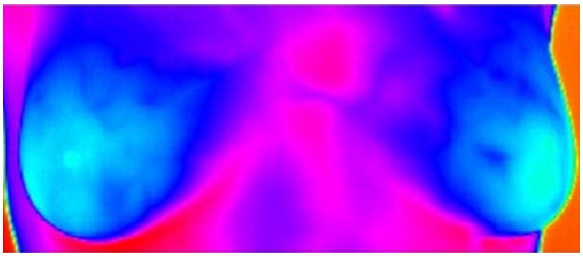

Registered LIR image after challenge

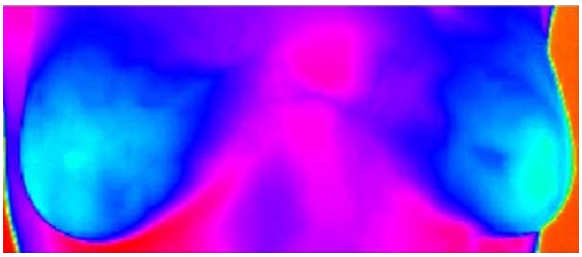

Registered LIR image before challenge

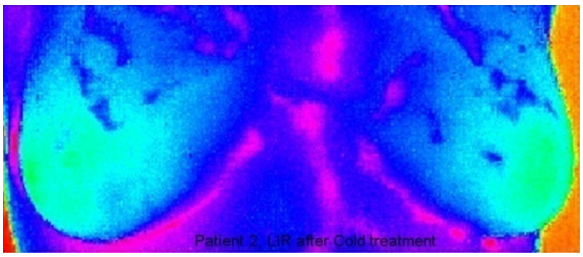

Image result with challenge after the LCNN process

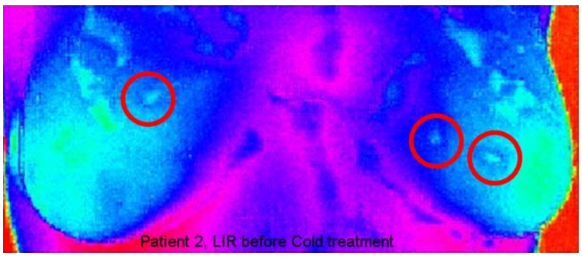

Image result without challenge after the LCNN process

Fig. 12 Simulation results of the LIR images with and without challenge using LCNN process

6. SKIN CANCER

Based on current estimates, 8,420 people are expected to die from melanoma in 2008 [1]. In an effort to reverse this sobering trend, dermatologists and the scientific community alike are continually developing new diagnostics, refining detection guidelines and providing patients with the tools they need to properly examine their own skin for signs of skin cancer. Recently, there are some exciting innovations in diagnosing skin cancer that can help us detect skin cancer early, when it is most treatable. The objective of this paper is to address a simple detection tool technology such that patients can use in their own homes can save thousands of lives."

Dermatologists traditionally diagnose skin cancer by evaluating the skin using a clinical examination and, if necessary, a magnifying device and then biopsying any suspicious lesions. Now, technological advances in computers, various sensor technologies and powerful digital signal processing are providing dermatologists with tools to enhance the evaluation of suspicious lesions and, in some cases, decreasing the number of biopsies needed for an accurate diagnosis. The idea is to hone in on suspicious lesions earlier and with more specificity. One of the newest technological developments in the fight against skin cancer is the use of sophisticated imaging to scan and enhance certain features of suspected lesions.

Similar to how a computerized tomography (CT) scan, but harmless highlights areas of the brain for abnormalities, imaging devices can now work on the skin to help detect cancerous tissue.

Skin lesion looks different and is changing in size, shape or color. Other qualities of moles for which individuals should check their skin include:

- Asymmetry – one half unlike the other half
- Border – irregular, scalloped or poorly defined
- Color – varies from one area to another; shades of tan and brown, black; sometimes white, red or blue
- Diameter – the size of a pencil eraser or larger

If a mole exhibits any of these characteristics, it should be brought to a dermatologist's attention. Typical skin lesions are displayed in Fig. 9.

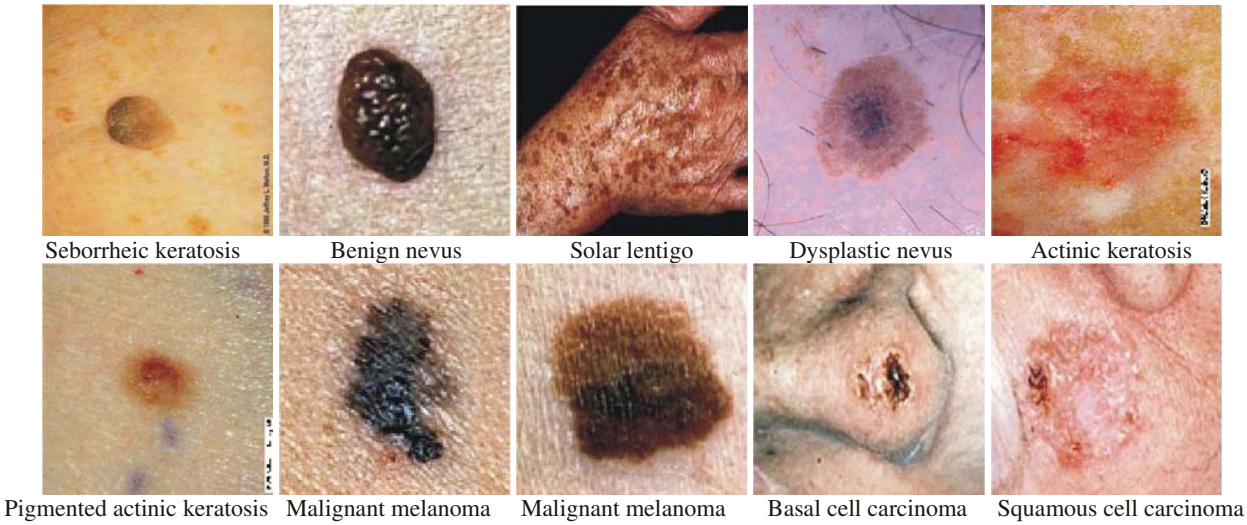

Fig.12 Typical skin lesions

Acknowledgement

We thank Dr. Felix Hong of Wayne State Medical School and Mr. Joseph Landa of Briartek Alexandria VA for actively participate our week long experiment in Birmingham as observers and have generously contributed to the project their insights.

REFERENCES

[1] Stuart Horn, Paul Norton, T. Cincotta, Andrew J. Stoltz, Jr., J. D. Benson, Philip Perconti, J. Campbell, "Challenges for third-Generation cooled imagers," Proc. SPIE Vol. 5074, p. 44-51, Infrared Technology and Applications XXIX; Bjorn F. Andresen, Gabor F. Fulop; Eds. Oct 2003.

[2] Paul R. Norton, James B. Campbell III, Stuart B. Horn, Donald A. Reago, "Third-Generation infrared imagers," Proc. SPIE Vol. 4130, p. 226-236, Infrared Technology and Applications XXVI; Bjorn F. Andresen, Gabor F. Fulop, Marija Strojnik; Eds., Dec 2000.

[3] John D. O'Connor, Ronald G. Driggers, Richard H. Vollmerhausen, Nicole M. Devitt, Jeff Olson, "Fifty-percent probability of identification (N50) comparison for targets in the visible and infrared spectral bands," Optical Engineering 42(10), p. 3047-3052, Oct 2003.

[4] Maes F., Collignon A., Vandermeulen D., Marchal G., Suetens P. (1997). Multimodality image registration by maximization of mutual information, IEEE transactions on Medical Imaging, vol. 16, no. 2, pp. 187-198, April 1997.

[5] Niederöst J. (2001). 3D reconstruction and accuracy analysis of historical relief models from the 18th century. 3rd International Image Sensing Seminar on New Development in Digital Photogrammetry, Gifu, Japan, 24+27 September 2001.

[6] Fraser C.S., Yamakawa T. (2003). Applicability of the affine model for Ikonos image orientation over mountainous terrain. Workshop on HRM from Space, 6-8 October, Hanover, 6p.

[7] H. Szu, L. Miao, and H. Qi, "Thermodynamic Free-energy Minimization for Unsupervised Fusion of Dual-color Infrared Breast Images," *Independent Component Analysis, Wavelets, Unsupervised Smart Sensors, and Neural Networks IV at SPIE Defense and Security Symposium*, Orlando, FL, Apr. 17-21, 2006.

[8] H. Szu and C. Hsu, "Landsat Spectral Demixing à la Superresolution of Blind Matrix Inversion by Constraint MaxEnt Neural Nets," in Wavelet Applications IV, Orlando FL.,H. Szu, Ed., *Proc. SPIE*, 3078, pp. 147-160.1997.